NANO LETTERS
Cite This: Nano Lett. 2018, 18, 734−739
Letter
pubs.acs.org/NanoLett

# Control over Electron−Phonon Interaction by Dirac Plasmon Engineering in the $Bi_2Se_3$ Topological Insulator

Chihun In,[†] Sangwan Sim,[†,§] Beom Kim,[†] Hyemin Bae,[†] Hyunseung Jung,[∥] Woosun Jang,[‡] Myungwoo Son,[⊥] Jisoo Moon,[#] Maryam Salehi,[▽] Seung Young Seo,[⊕] Aloysius Soon,[‡] Moon-Ho Ham,[⊥] Hojin Lee,[∥] Seongshik Oh,[#,○] Dohun Kim,[◆] Moon-Ho Jo,[§,¶,⊕] and Hyunyong Choi*[,†]

[†]School of Electrical and Electronic Engineering and [‡]Department of Materials Science and Engineering, Yonsei University, Seoul 03722, Republic of Korea

[§]Center for Artificial Low Dimensional Electronic Systems, Institute for Basic Science (IBS), Pohang 37673, Republic of Korea

[∥]School of Electronic Engineering, Soongsil University, Seoul 06978, Republic of Korea

[⊥]School of Materials Science and Engineering, Gwangju Institute of Science and Technology (GIST), Gwangju 61005, Republic of Korea

[#]Department of Physics and Astronomy, [▽]Department of Materials Science and Engineering, and [○]Institute for Advanced Materials, Devices and Nanotechnology, Rutgers University, Piscataway, New Jersey 08854, United States

[◆]Department of Physics and Astronomy, Seoul National University, Seoul 08826, Republic of Korea

[¶]Division of Advanced Materials Science and [⊕]Department of Materials Science and Engineering, Pohang University of Science and Technology (POSTECH), Pohang 37673, Republic of Korea

Supporting Information

**ABSTRACT:** Understanding the mutual interaction between electronic excitations and lattice vibrations is key for understanding electronic transport and optoelectronic phenomena. Dynamic manipulation of such interaction is elusive because it requires varying the material composition on the atomic level. In turn, recent studies on topological insulators (TIs) have revealed the coexistence of a strong phonon resonance and topologically protected Dirac plasmon, both in the terahertz (THz) frequency range. Here, using these intrinsic characteristics of TIs, we demonstrate a new methodology for controlling electron−phonon interaction by lithographically engineered Dirac surface plasmons in the $Bi_2Se_3$ TI. Through a series of time-domain and time-resolved ultrafast THz measurements, we show that, when the Dirac plasmon energy is less than the TI phonon energy, the electron−phonon coupling is trivial, exhibiting phonon broadening associated with Landau damping. In contrast, when the Dirac plasmon energy exceeds that of the phonon resonance, we observe suppressed electron−phonon interaction leading to unexpected phonon stiffening. Time-dependent analysis of the Dirac plasmon behavior, phonon broadening, and phonon stiffening reveals a transition between the distinct dynamics corresponding to the two regimes as the Dirac plasmon resonance moves across the TI phonon resonance, which demonstrates the capability of Dirac plasmon control. Our results suggest that the engineering of Dirac plasmons provides a new alternative for controlling the dynamic interaction between Dirac carriers and phonons.

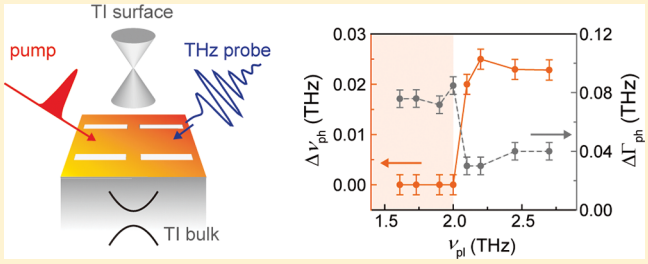


**KEYWORDS:** *Topological insulators, plasmon, phonon, terahertz, ultrafast*

Topological insulators (TIs) are intriguing quantum materials exhibiting topologically protected surface Dirac states with suppressed elastic backscattering at an angle of $\pi$.[1−4] At elevated temperature, the electrical transport other than the scattering at an angle of $\pi$ results in a finite conductivity primarily limited by the scattering of Dirac carriers with phonons.[5−7] Therefore, it is of fundamental importance to investigate such interactions for determining the fundamental operation limits of TI-based devices.[8−13] For materials with Dirac carrier transport such as graphene, whose linear dispersion resembles the surface states of TIs, theories have shown that it is indeed possible to exploit electric or optical means to control the coupling between Dirac Fermions and phonons.[14] For experimental demonstration, the interaction between the continuum-like Dirac Fermions and the discrete

**Received:** September 11, 2017
**Revised:** January 9, 2018
**Published:** January 18, 2018





DOI: 10.1021/acs.nanolett.7b03897
Nano Lett. 2018, 18, 734−739

high-energy optical phonons (~200 meV) was manipulated by switching the Landau damping kinetics of the $G$ phonon using either electrostatic gating[15] or nonequilibrium optical excitation.[16] Although this approach is promising, the control of phonon decay into particle−hole pairs via Landau damping is a daunting task in TIs because even the strongest long-wavelength optical phonon (the $\alpha$ mode at ~1.9 THz) is well-within the energy range of several meV,[4,17−19] such that the control (field-effect-based or optical) of the electron−phonon interaction is easily screened by continuum-like THz Drude responses, especially at elevated temperatures due to the thermal excitation of free carriers.

In this Letter, we report on an alternative approach for manipulating the pathways of the interaction between Dirac carriers and phonons. Inspired by recent theoretical predictions[20−25] and experimental demonstrations[9,26−32] of two-dimensional (2D) Dirac plasmons in TIs, we show that the damping and resonance energy of phonons can be controlled by tuning the 2D Dirac plasmon resonance. We find that, when the energy of the quasi-resonant 2D Dirac plasmon is below that of the $\alpha$ mode 1.9 THz phonon, the phonon experiences Landau damping, resulting in trivial broadening of the phonon resonance without noticeable energy shifts. When the energy of the Dirac plasmon resonance is increased to exceed the $\alpha$ mode phonon energy, we observe a surprising phenomenon, namely phonon stiffening accompanied by a reduction in the phonon broadening. Our ultrafast THz study reveals that the two intriguing features are complementary, further confirming that the electron−phonon interaction can be effectively controlled by the 2D Dirac plasmon engineering.

Samples of TI $Bi_2Se_3$ thin films with 25 quintuple layers (QLs) and 15 QLs were synthesized on 0.5 mm thick sapphire ($Al_2O_3$) substrates by molecular beam epitaxy.[33] Dirac plasmons were achieved by fabricating arrays of slits or rods using standard photolithography (Supporting Information section A). Figure 1a displays the periodically arranged slits with 25 QL $Bi_2Se_3$ and rods with 15 QL $Bi_2Se_3$ fabricated by UV lithography and reactive ion etching.[9,27] The length $L$ of slits or rods was varied from 14 to 5 $\mu$m to create an additional momentum of $k \approx \pi/L$ required for plasmon excitation.[9] The spacing $W$ was fixed at 4 $\mu$m, and the side of the corresponding unit cell was defined as $L + W$. For ultrafast THz measurements, we used a 250 kHz Ti/sapphire regenerative amplifier (Coherent RegA 9050) to generate 50 fs ultrashort pulses with a photon energy of 1.55 eV. Picosecond (ps) THz pulses were generated by optical rectification in a < 110>-oriented ZnTe single crystal, and the THz pulses transmitted through the sample were detected by electro-optic sampling in an additional pair of <110>-oriented ZnTe. A part of the 1.55 eV laser output was used for optical excitation.[27]

We first measure the Fourier-transformed transmittance $T(\nu)$ of the patterned TI structures using THz time-domain spectroscopy at a temperature of 78 K. The corresponding THz extinction spectra $E(\nu)=1 - T(\nu)$ are shown in Figure 1b, where the polarization of the THz electric field is perpendicular (parallel) to the length of the slit (rod) to match the direction of the reciprocal lattice vectors of the plasmon excitation. According to the Babinet's principle, a slit supports an "anti-dipole" resonance for perpendicularly polarized light, given that the corresponding rod is resonant along the dipole direction.[30] Indeed, the $E(\nu)$ spectra of slits and rods are quite similar for the same length $L$. The $E(\nu)$ spectra are composed of a nearly discrete resonance of the $\alpha$ mode phonon and a broad quasi-

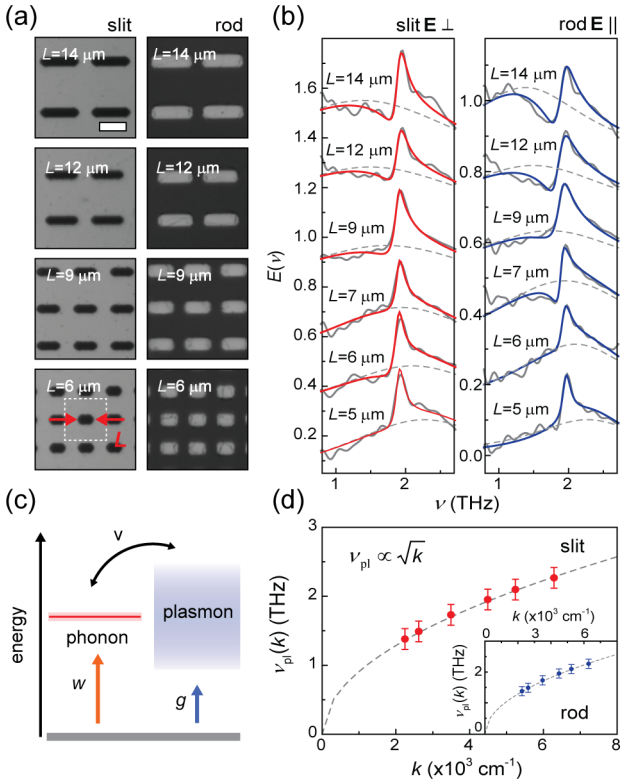


**Figure 1.** (a) Optical microscope images of the fabricated TI plasmonic structures with arrays of slits or rods with a length of $L$. (b) THz extinction spectra $E(\nu)$ for different $L$ measured at $T$ = 78 K. The polarization of the incident THz electric field is perpendicular (parallel) to the direction of the slit (rod). Gray solid lines are experimentally measured values, and red and blue lines are fits obtained from the Fano model. Gray dashed lines are the spectra of the bare plasmon without the Fano interference. (c) Schematic illustration of the energy diagram representing the Fano interference with parameters v, $w$, and $g$. A discrete energy level of the optical phonon $\hbar\omega_{ph}$ and quasi-resonant plasmon $\hbar\omega_{pl}$ are shown. (d) Plasmon frequency $\nu_{pl}$ of the TI slits as a function of wavevector $k$ (red solid dots), together with a fit to the data (gray dashed line). The inset shows the $\nu_{pl}$ for the TI rods (blue solid dots) together with the fit corresponding to the TI slits (gray dashed line).

resonant plasmon peak, which gradually shifts toward higher frequencies with decreasing $L$. In the patterned TI plasmonic structures, these two different resonances lead to Fano-like quantum interference.[9,27] To obtain the phonon ($\nu_{ph}$) and bare plasmon ($\nu_{pl}$) frequencies, we fit the data in Figure 1b using a Fano model derived from the energy diagram in Figure 1c (Supporting Information section B). Here, the parameter $w$ ($g$) is the factor describing a coupling between incident photons and the phonon (plasmon), which gives rise to typical Lorentz extinction spectra, while $v$ determines the Fano interference between the plasmon and phonon.[34,35]

In Figure 1b, we also show in the same plot the bare plasmon spectrum with a gray dashed line (Supporting Information section C). As demonstrated by Stauber et al.,[20−22] the relationship between $\nu_{pl}$ and $k$ is important for understanding the properties of the 2D Dirac plasmon; theoretical and experimental investigations[9] show that $\nu_{pl}$ is proportional to the square root of $k$. The plasmon dispersion in Figure 1d confirms that plasmons in TI slits and rods indeed originate from a 2D Dirac electronic system. Unlike the case of graphene, both massless Dirac Fermions and massive particles in the 2D



DOI: 10.1021/acs.nanolett.7b03897
Nano Lett. 2018, 18, 734−739

electron gas (2DEG) constitute plasmons in TI. The densities of massless Dirac carriers $n_{Dirac} \approx 1.1 \times 10^{13}$ cm$^{-2}$ and massive 2DEG particles $n_{2DEG} = 2.2 \times 10^{12}$ cm$^{-2}$ extracted from the plasmon dispersion (Supporting Information section D) are consistent with the results of previous angle-resolved photoemission measurements.[36] We note that the line width of the plasmon resonance does not show a strong dependence on $\nu_{pl}$ (Supporting Information section C), indicating that, unlike in the case of graphene plasmons[37] or metal nanoparticles,[38] the damping of the TI plasmon due to edge scattering is negligible in our TI plasmonic structures.

With the confirmed excitation of 2D Dirac plasmons in our patterned TI structures, we now investigate the dynamic interaction between the plasmon and phonon resonances through measuring the pump-induced changes of extinction spectra $\Delta E(\nu)$. As seen in Figure 2a, the transient THz dynamics, $E_{THz}/E_0$, exhibits a relaxation time of a few ps after pump excitation with a fluence of $F = 35$ $\mu$J/cm$^2$. Positive values of $E_{THz}/E_0$ lead to positive changes $\Delta E(\nu)$ and, thereby, a transient increase in $n_{Dirac}$ and $n_{2DEG}$ (Figure 2b). The broad $\Delta E(\nu)$ spectrum away from the $\alpha$ mode 1.9 THz phonon is positive for all samples, which is associated with the pump-induced photocarrier generation.[27] After fitting the spectra $\Delta E(\nu)$ in Figure 2b with the Fano model described in Supporting Information section E, we plot in Figure 2c the transient plasmon dispersion after optical excitation. As discussed in previous studies,[22,27] optical excitation of trivial bulk states is responsible for the blue-shift of $\nu_{pl}$. The plasmon dispersion after optical excitation yields the increased 2DEG densities $\Delta n_{2DEG} \approx 7.3 \times 10^{12}$ cm$^{-2}$ at $\Delta t$ of 6 ps (Supporting Information section F). We note that, in Figures 2b,c, the $\Delta E(\nu)$ spectra are symmetric (asymmetric) for the values of $L$ from 14 to 9 $\mu$m (from 8 to 5 $\mu$m) near the $\alpha$ mode 1.9 THz phonon resonance. Here, the transient values of $\nu_{pl}$ for $L$ from 14 to 9 $\mu$m are below 2.0 THz, while those for $L$ from 8 to 5 $\mu$m are above 2.1 THz. Given that the $\alpha$ mode phonon is at ~1.9 THz, it is intriguing that the transient phonon dynamics are strongly correlated with the frequency $\nu_{pl}$ of the 2D Dirac plasmon resonance.

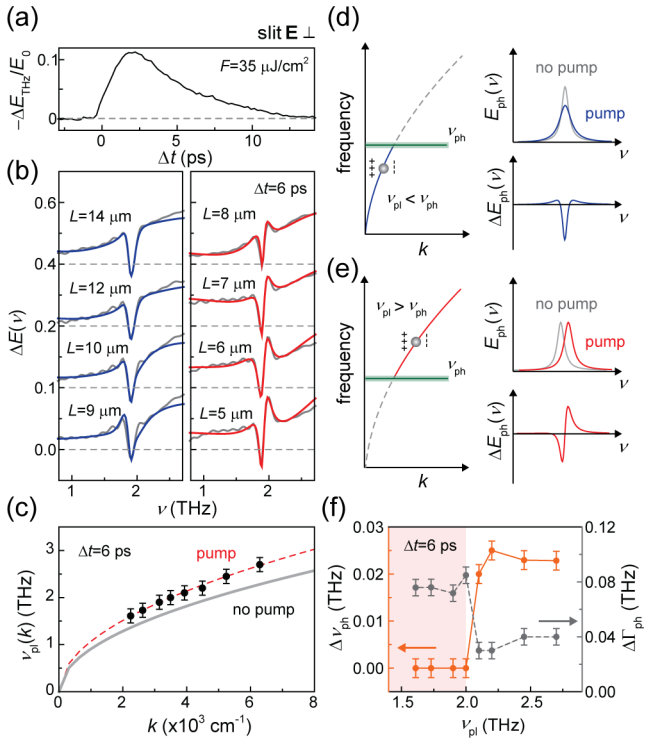


**Figure 2.** (a) Pump-induced change in the transmitted THz electric field, $\Delta E_{THz}/E_0$, as a function of $\Delta t$. (b) Changes in THz extinction spectra $\Delta E(\nu)$ are measured in TI slits with different $L$. Blue and red solid lines are fits obtained from the Fano model. Gray dashed lines indicate $\Delta E(\nu) = 0$. The experimental data were obtained at a temperature of $T = 78$ K and pump−probe delay of $\Delta t = 6$ ps. (c) $\nu_{pl}$ as a function of $k$ at $\Delta t = 6$ ps (black dots) together with a fit (red dashed). A solid gray line is a fit from Figure 1d. (d,e) Left: the frequency dispersion of the plasmon and optical phonon as functions of $k$. Right: schematic illustration of phonon broadening (blue lines) and phonon stiffening (red lines). Gray lines in $E_{ph}(\nu)$ indicate the phonon resonance at equilibrium, and the colored lines in $E_{ph}(\nu)$ indicate the phonon resonance after optical excitation. The corresponding changes in the phonon resonance $E_{ph}(\nu)$ are shown in the plots below. (f) Transient phonon frequency $\Delta\nu_{ph}$ and phonon line width $\Delta\Gamma_{ph}$ as functions of $\nu_{pl}$ at $\Delta t = 6$ ps.

The different $\Delta E(\nu)$ spectra can be explained schematically by displaying the plasmon and phonon dispersion curves as shown in Figure 2d for $\nu_{pl} < \nu_{ph}$ and in Figure 2e for $\nu_{pl} > \nu_{ph}$. The corresponding bare phonon extinction spectra $E_{ph}(\nu)$ and their variations $\Delta E_{ph}(\nu)$ are also shown. Here, the branch of the $\alpha$ mode optical phonon is indicated by a horizontal line because its dispersion in the THz range is almost $k$-independent compared to that of the 2D Dirac plasmon.[39,40] Figure 2d illustrates that the increased phonon line width $\Gamma_{ph}$ results in a symmetric shape of $\Delta E_{ph}(\nu)$; thus, "phonon broadening" accounts for the dynamic states of the phonon when $\nu_{pl} < \nu_{ph}$. However, the increased $\nu_{ph}$ in Figure 2e is expected to result in an asymmetric shape of $\Delta E_{ph}(\nu)$; therefore, the phonon dynamics for $\nu_{pl} > \nu_{ph}$ can be explained by "phonon stiffening". Here, we emphasize that the asymmetric shape of $\Delta E_{ph}(\nu)$ in Figure 2b is not the result of Fano-like interference. We note that, even when we change the Fano coupling parameter $\nu$, the asymmetric $\Delta E_{ph}(\nu)$ spectra cannot be reproduced (Supporting Information section E). Figure 2f summarizes these dynamics in our TI plasmonic structures, in which the changes in phonon frequency $\Delta\nu_{ph}$ and line width $\Delta\Gamma_{ph}$ are displayed. When $\nu_{pl} < \nu_{ph}$, a significant $\Delta\Gamma_{ph}$ is clearly observed with negligible $\Delta\nu_{ph}$. However, when $\nu_{pl}$ exceeds $\nu_{ph}$, we see a rapid drop of $\Delta\Gamma_{ph}$ and increased $\Delta\nu_{ph}$ above 0.02 THz. The hyperbolic phonon polaritons located at 1.9 THz and 4.1 THz could possibly contribute to the dynamic interaction between the Dirac plasmon and the phonon.[23,24] However, our electromagnetic simulations for variable density and temperature show that such contribution is marginal due to the significantly increased optical loss near 1.9 THz (Supporting Information section G). To distinguish the contribution of the hyperbolic phonon polaritons, a more-direct experimental method such as a scattering-type near-field scanning optical microscopy is required.[41−44]

The sharp transformation across the $\alpha$ mode 1.9 THz phonon might be reminiscent of the Landau damping of optical phonons via the electron−hole pair excitation in graphene.[14−16] In this case, the coupling of the phonon and Dirac Fermions shows increased damping of the phonon and renormalization of the phonon energy. The shadowed region in Figure 2f indicates the Landau damping regime for the $\alpha$-mode phonon. In contrast to the case of graphene, in which the Landau damping of the high-energy $G$ phonon explicitly contributes to the electron−hole pair excitation,[15] there is no such contribution associated with the TI $\alpha$-mode phonon. This is because the


DOI: 10.1021/acs.nanolett.7b03897
Nano Lett. 2018, 18, 734−739

Fermi level of our TI is hundreds of times higher than the $\alpha$-mode phonon energy, such that the effect of the increased phase space for the Dirac plasmons to be scattered due to the optical illumination is negligible. We have shown theoretically that the renormalized phonon self-energy based on a graphene theory is indeed not applicable to the decay dynamics of the TI $\alpha$-mode phonon. Instead, as shown by our numerical simulations based on a plasma theory (see more details in Supporting Information section H), the time-dependent changes of $\Delta\nu_{ph}$ and $\Delta\Gamma_{ph}$ originate from the screening effect of an incoherent electron plasma and thereby are strongly affected by the Dirac plasmon momentum $k$ and the corresponding resonance energy.

The two different regimes are illustrated schematically in Figure 3a, where the left panel represents the case of the engineered 2D Dirac plasmon with $\nu_{pl} < \nu_{ph}$, and the right panel corresponds to $\nu_{pl} > \nu_{ph}$. To further investigate the dynamic interaction between the 2D Dirac plasmon and phonon at different $\Delta t$, we perform time-resolved THz spectroscopy with two preferentially selected TI slits with $L = 12$ $\mu$m ($S_{12}$) and $L = 6$ $\mu$m ($S_6$), with the results shown in Figure 3b. The time-resolved $\Delta E(\nu)$ spectra in Figure 3b are also composed of broad extinction peaks of the 2D Dirac plasmon and sharp phonon extinction features, similar to the $\Delta E(\nu)$ spectra in Figure 2b. The rising shape of $\Delta E(\nu)$ with increasing frequency implies a blue-shift of $\nu_{pl}$; the corresponding plasmon excitation relaxes within several picoseconds as the optically excited electrons are recombined. Employing the Fano model used earlier, we extract the plasmon frequencies $\nu_{pl}$ of the two samples as functions of $\Delta t$ (Supporting Information section E), and the results are shown in Figure 3c. There, we see that $\nu_{pl}$ in $S_{12}$ ($S_6$) is lower (higher) than $\nu_{ph}$ for all $\Delta t$. Given that $\nu_{ph}$ is at ~1.9 THz, $\nu_{pl}$ for $S_{12}$ is always lower than $\nu_{ph}$, even for early $\Delta t$. The relaxation dynamics of $\nu_{pl}$ is quite similar for $S_{12}$ and $S_6$, which suggests that the change in $\nu_{pl}$ after optical excitation can be attributed to the intrinsic nonequilibrium Dirac Fermion relaxation of TIs.[45] Indeed, the time-dependent $\Delta n_{2DEG}$ in the inset of Figure 3c, obtained from the 2D Dirac plasmon dispersion, closely follows the relaxation dynamics of $-E_{THz}/E_0$ presented in Figure 2a.

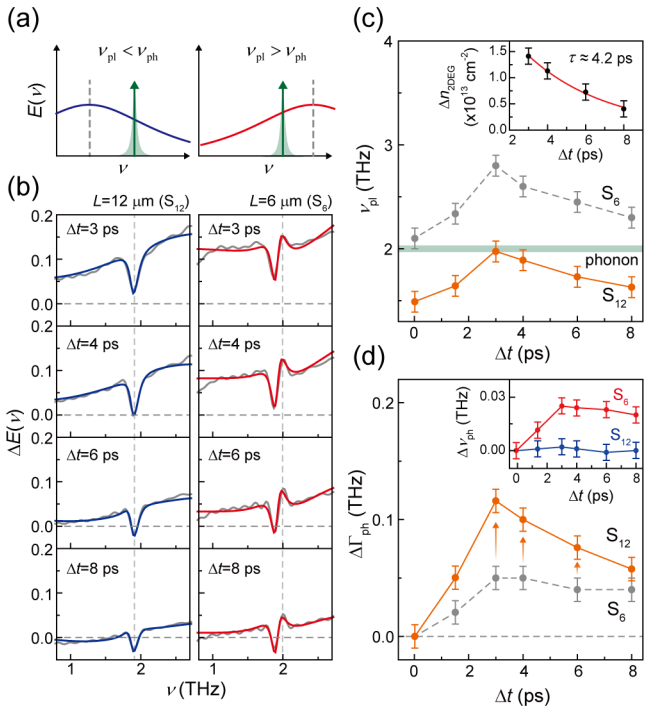


**Figure 3.** (a) Schematics of the plasmon and phonon spectra $E(\nu)$ for $\nu_{pl} < \nu_{ph}$ (left) and $\nu_{pl} > \nu_{ph}$ (right). (b) Time-resolved $\Delta E(\nu)$ dynamics for $\Delta t$ from 3 to 8 ps for TI slits with $L = 12$ $\mu$m ($S_{12}$, left) and $L = 6$ $\mu$m ($S_6$, right). Gray solid lines are experimentally measured values, while blue and red lines are fits to the data. Vertical dashed lines indicate the phonon resonances after optical excitation. (c) Dynamics of $\nu_{pl}$ for $S_{12}$ (orange dots) and $S_6$ (gray dots). The inset shows the changes in the 2DEG density $\Delta n_{2DEG}$. (d) Transient phonon line width $\Delta\Gamma_{ph}$ for $S_{12}$ (orange dots) and $S_6$ (gray dots). Inset: transient phonon frequency $\Delta\nu_{ph}$ for $S_{12}$ (blue dots) and $S_6$ (red dots).

We now discuss the time-dependent dynamics of $\Delta\nu_{ph}$ and $\Delta\Gamma_{ph}$ for $S_{12}$ and $S_6$. Figure 3d shows the dynamics of the phonon damping for $S_{12}$ and $S_6$. The phonon line width for $S_{12}$ is always larger than that for $S_6$ at all $\Delta t$ (in Supporting Information section H, we present the detailed theoretical investigation of the phonon Landau damping due to the increase in the 2DEG density $n_{2DEG}$ and the increased electron temperature $T_e$). As predicted theoretically,[20−22] the band-bending-induced 2D electron is the main contributor. This is also supported by the fact that the relaxation time of $\Delta\Gamma_{ph}$ for $S_{12}$ is ~4 ps, very similar to the time constant of optically excited 2DEG (see the inset of Figure 3c). For $S_6$, because the Landau damping is less effective than for $S_{12}$, both $\Delta\Gamma_{ph}$ and $\Delta\nu_{ph}$ should differ from the corresponding values for $S_{12}$. In fact, the transient $\Delta\Gamma_{ph}$ for $S_6$ exhibits a much-longer relaxation time (~21 ps) than for $S_{12}$ and reaches only ~0.06 THz at its maximum. This small but finite $\Delta\Gamma_{ph}$ in $S_6$ can be understood as the increased lattice temperature $T_L$ after optical excitation.[17,46] According to a simple two-temperature model (Supporting Information section I), optical excitation leads to a rapid increase of $T_e$ reaching above 1,100 K at $F = 35$ $\mu$J/cm$^2$, and the subsequent cooling and decrease of $T_e$ result in the increased $T_L$. Consequently, the cooling dynamics of the hot phonon may dominate the slow $\Delta\Gamma_{ph}$ transients. This scenario is also supported by the $\Delta\nu_{ph}$ dynamics, as shown in the inset of Figure 3d. A clear signature of phonon stiffening is visible only for $S_6$. Switching off the Landau damping renders $S_6$ a less-coupled system in terms of the electron−phonon interaction. The similar long relaxation time of ~21 ps for $\Delta\nu_{ph}$ and $\Delta\Gamma_{ph}$ in $S_6$ indicates that its temporal dynamics is different from the case of $S_{12}$.

In conclusion, we demonstrate that the interaction between Dirac carriers and phonons can be controlled by engineering the 2D Dirac plasmon resonance $\nu_{pl}$. When $\nu_{pl}$ is lower than $\nu_{ph}$, the phonon broadening is dominant in the observed transient $\Delta E(\nu)$ spectra. The increase in $\Gamma_{ph}$ implies Landau damping of the phonon through the electron−phonon coupling. In contrast, when $\nu_{pl}$ is higher than $\nu_{ph}$, suppressed electron−phonon coupling is observed, resulting in the phonon stiffening. Our observations indicate that the coupling of electrons and phonons can be significantly different depending on the properties of the 2D Dirac plasmons, which is potentially beneficial for TI-based electronics and TI plasmonic applications.



DOI: 10.1021/acs.nanolett.7b03897
Nano Lett. 2018, 18, 734−739

## ■ ASSOCIATED CONTENT

### Supporting Information

The Supporting Information is available free of charge on the ACS Publications website at DOI: 10.1021/acs.nanolett.7b03897.

Additional information on sample preparation, equations for spectral fitting, spectral fitting results and plasmon dispersion at equilibrium and non-equilibrium, hyperbolic plasmon−phonon polaritons, phonon Landau damping, hot phonon dynamics, and fit constants. (PDF)

## ■ AUTHOR INFORMATION


### Corresponding Author

*E-mail: hychoi@yonsei.ac.kr.

### ORCID

Woosun Jang: 0000-0003-1274-1714
Aloysius Soon: 0000-0002-6273-9324
Moon-Ho Ham: 0000-0001-5862-6012
Seongshik Oh: 0000-0003-1681-516X
Moon-Ho Jo: 0000-0002-3160-358X
Hyunyong Choi: 0000-0003-3295-1049


### Notes

The authors declare no competing financial interest.

## ■ ACKNOWLEDGMENTS

C.I., S.S., B.K., H.B., and H.C. were supported by the National Research Foundation of Korea (NRF) through the government of Korea (MSIP) (grant nos. NRF-2016R1A4A1012929 and NRF-2015R1A2A1A10052520) and the Global Frontier Program (grant no. 2014M3A6B3063709). H.J., W.J., M.S., A.S., M.-H.H., and H.L. were supported by NRF through MSIP (grant no. NRF-2016R1A4A1012929). C.I., S.S., B.K., H.B., M.S., M.-H.H., and H.C. were supported by Creative Materials Discovery Program through the National Research Foundation of Korea (NRF) funded by the Ministry of Science and ICT (grant no. 2017M3D1A1040828). C.I. was supported by NRF through MSIP (grant no. NRF-2015H1A2A1034809). J.M., M.S., and S.O. were supported by Gordon and Betty Moore Foundation's EPiQS Initiative (grant no. GBMF4418) and the National Science Foundation (NSF) (grant no. EFMA-1542798). S.Y.S. and M.-H.J. were supported by the Institute for Basic Science (IBS), Korea, under the Project Code no. IBS-R014-A1-2017-a00.

## ■ REFERENCES


(1) Hasan, M. Z.; Kane, C. L. Colloquium: Topological insulators. *Rev. Mod. Phys.* **2010**, *82* (4), 3045−3067.

(2) Lee, C.; Katmis, F.; Jarillo-herrero, P.; Moodera, J. S.; Gedik, N. Direct measurement of proximity-induced magnetism at the buried interface between a topological insulator and a ferromagnet. *Nat. Commun.* **2016**, *7*, 12014.

(3) Bowlan, P.; Bowlan, J.; Trugman, S. A.; Valdés Aguilar, R.; Qi, J.; Liu, X.; Furdyna, J.; Dobrowolska, M.; Taylor, A. J.; Yarotski, D. A.; Prasankumar, R. P. Probing and controlling terahertz-driven structural dynamics with surface sensitivity. *Optica* **2017**, *4* (3), 383−387.

(4) Wu, L.; Tse, W. K.; Brahlek, M.; Morris, C. M.; Aguilar, R. V.; Koirala, N.; Oh, S.; Armitage, N. P. High-resolution Faraday rotation and electron-phonon coupling in surface states of the bulk-insulating topological insulator $Cu_{0.02}Bi_2Se_3$. *Phys. Rev. Lett.* **2015**, *115* (21), 217602.

(5) Kim, D.; Li, Q.; Syers, P.; Butch, N. P.; Paglione, J.; Sarma, S. D.; Fuhrer, M. S. Intrinsic electron-phonon resistivity of $Bi_2Se_3$ in the topological regime. *Phys. Rev. Lett.* **2012**, *109* (16), 166801.

(6) Costache, M. V.; Neumann, I.; Sierra, J. F.; Marinova, V.; Gospodinov, M. M.; Roche, S.; Valenzuela, S. O. Fingerprints of inelastic transport at the surface of the topological insulator $Bi_2Se_3$: Role of electron-phonon coupling. *Phys. Rev. Lett.* **2014**, *112*, 086601.

(7) Luo, C. W.; Wang, H. J.; Ku, S. A.; Chen, H. J.; Yeh, T. T.; Lin, J. Y.; Wu, K. H.; Juang, J. Y.; Young, B. L.; Kobayashi, T.; Cheng, C. M.; Chen, C. H.; Tsuei, K. D.; Sankar, R.; Chou, F. C.; Kokh, K. A.; Tereshchenko, O. E.; Chulkov, E. V.; Andreev, Y. M.; Gu, G. D. Snapshots of Dirac fermions near the Dirac point in topological insulators. *Nano Lett.* **2013**, *13* (12), 5797−5802.

(8) Valdes Aguilar, R.; Stier, A. V.; Liu, W.; Bilbro, L. S.; George, D. K.; Bansal, N.; Wu, L.; Cerne, J.; Markelz, A. G.; Oh, S.; et al. Armitage, N. P. Terahertz response and colossal Kerr rotation from the surface states of the topological insulator $Bi_2Se_3$. *Phys. Rev. Lett.* **2012**, *108* (8), 087403.

(9) Di Pietro, P.; Ortolani, M.; Limaj, O.; Di Gaspare, A.; Giliberti, V.; Giorgianni, F.; Brahlek, M.; Bansal, N.; Koirala, N.; Oh, S.; Calvani, P.; Lupi, S. Observation of Dirac plasmons in a topological insulator. *Nat. Nanotechnol.* **2013**, *8* (8), 556−560.

(10) Wang, Y.; Deorani, P.; Banerjee, K.; Koirala, N.; Brahlek, M.; Oh, S.; Yang, H. Topological surface states originated spin-orbit torques in $Bi_2Se_3$. *Phys. Rev. Lett.* **2015**, *114* (25), 257202.

(11) Slobozhanyuk, A. P.; Poddubny, A. N.; Miroshnichenko, A. E.; Belov, P. A.; Kivshar, Y. S. Subwavelength topological edge states in optically resonant dielectric structures. *Phys. Rev. Lett.* **2015**, *114* (12), 123901.

(12) Gubbin, C. R.; Martini, F.; Politi, A.; Maier, S. A.; De Liberato, S. Strong and coherent coupling between localized and propagating phonon polaritons. *Phys. Rev. Lett.* **2016**, *116* (24), 246402.

(13) Wang, D.; Yang, A.; Wang, W.; Hua, Y.; Schaller, R. D.; Schatz, G. C.; Odom, T. W. Band-edge engineering for controlled multi-modal nanolasing in plasmonic superlattices. *Nat. Nanotechnol.* **2017**, *12* (9), 889−894.

(14) Ando, T. Anomaly of optical phonon in monolayer graphene. *J. Phys. Soc. Jpn.* **2006**, *75* (12), 124701.

(15) Yan, J.; Zhang, Y.; Kim, P.; Pinczuk, A. Electric field effect tuning of electron-phonon coupling in graphene. *Phys. Rev. Lett.* **2007**, *98* (16), 166802.

(16) Yan, H.; Song, D.; Mak, K. F.; Chatzakis, I.; Maultzsch, J.; Heinz, T. F. Time-resolved Raman spectroscopy of optical phonons in graphite: Phonon anharmonic coupling and anomalous stiffening. *Phys. Rev. B: Condens. Matter Mater. Phys.* **2009**, *80* (12), 121403.

(17) Sim, S.; Brahlek, M.; Koirala, N.; Cha, S.; Oh, S.; Choi, H. Ultrafast terahertz dynamics of hot Dirac-electron surface scattering in the topological insulator $Bi_2Se_3$. *Phys. Rev. B: Condens. Matter Mater. Phys.* **2014**, *89* (16), 165137.

(18) Sim, S.; Koirala, N.; Brahlek, M.; Sung, J. H.; Park, J.; Cha, S.; Jo, M. H.; Oh, S.; Choi, H. Tunable Fano quantum-interference dynamics using a topological phase transition in $(Bi_{1-x}In_x)_2Se_3$. *Phys. Rev. B: Condens. Matter Mater. Phys.* **2015**, *91* (23), 235438.

(19) Sim, S.; Park, J.; Koirala, N.; Lee, S.; Brahlek, M.; Moon, J.; Salehi, M.; Kim, J.; Cha, S.; Sung, J. H.; Jo, M. H.; Oh, S.; Choi, H. Composition control of plasmon-phonon interaction using topological quantum-phase transition in photoexcited $(Bi_{1-x}In_x)_2Se_3$. *ACS Photonics* **2016**, *3* (8), 1426−1431.

(20) Stauber, T.; Gómez-Santos, G.; Brey, L. Plasmonics in topological insulators: Spin-charge separation and the influence of the inversion layer. *ACS Photonics* **2017**, *4* (12), 2978−2988.

(21) Stauber, T.; Gómez-Santos, G.; Brey, L. Spin-charge separation of plasmonic excitations in thin topological insulators. *Phys. Rev. B: Condens. Matter Mater. Phys.* **2013**, *88* (20), 205427.

(22) Stauber, T. Plasmonics in Dirac systems: From graphene to topological insulators. *J. Phys.: Condens. Matter* **2014**, *26* (12), 123201.

(23) Basov, D. N.; Fogler, M. M.; Garcia de Abajo, F. J. Polaritons in van der waals materials. *Science* **2016**, *354* (6309), aag1992.




DOI: 10.1021/acs.nanolett.7b03897
*Nano Lett.* 2018, 18, 734−739

(24) Wu, J. S.; Basov, D. N.; Fogler, M. M. Topological insulators are tunable waveguides for hyperbolic polaritons. *Phys. Rev. B: Condens. Matter Mater. Phys.* **2015**, *92* (20), 205430.
(25) Profumo, R. E. V.; Asgari, R.; Polini, M.; MacDonald, A. H. Double-layer graphene and topological insulator thin-film plasmons. *Phys. Rev. B: Condens. Matter Mater. Phys.* **2012**, *85* (8), 085443.
(26) Autore, M.; D'Apuzzo, F.; Di Gaspare, A.; Giliberti, V.; Limaj, O.; Roy, P.; Brahlek, M.; Koirala, N.; Oh, S.; García de Abajo, F. J.; Lupi, S. Plasmon-phonon interactions in topological insulator microrings. *Adv. Opt. Mater.* **2015**, *3* (9), 1257−1263.
(27) Sim, S.; Jang, H.; Koirala, N.; Brahlek, M.; Moon, J.; Sung, J. H.; Park, J.; Cha, S.; Oh, S.; Jo, M.-H.; Ahn, J.-H.; Choi, H. Ultra-high modulation depth exceeding 2,400% in optically controlled topological surface plasmons. *Nat. Commun.* **2015**, *6*, 8814.
(28) Politano, A.; Silkin, V. M.; Nechaev, I. A.; Vitiello, M. S.; Viti, L.; Aliev, Z. S.; Babanly, M. B.; Chiarello, G.; Echenique, P. M.; Chulkov, E. V. Interplay of surface and Dirac plasmons in topological insulators: The case of $Bi_2Se_3$. *Phys. Rev. Lett.* **2015**, *115* (21), 216802.
(29) Kogar, A.; Vig, S.; Thaler, A.; Wong, M. H.; Xiao, Y.; Reig-I-Plessis, D.; Cho, G. Y.; Valla, T.; Pan, Z.; Schneeloch, J.; Zhong, R.; Gu, G. D.; Hughes, T. L.; Macdougall, G. J.; Chiang, T. C.; Abbamonte, P. Surface collective modes in the topological insulators $Bi_2Se_3$ and $Bi_{0.5}Sb_{1.5}Te_{3-x}Se_x$. *Phys. Rev. Lett.* **2015**, *115* (25), 257402.
(30) Ou, J.-Y.; So, J.-K.; Adamo, G.; Sulaev, A.; Wang, L.; Zheludev, N. I. Ultraviolet and visible range plasmonics in the topological insulator $Bi_{1.5}Sb_{0.5}Te_{1.8}Se_{1.2}$. *Nat. Commun.* **2014**, *5*, 5139.
(31) Dubrovkin, A. M.; Adamo, G.; Yin, J.; Wang, L.; Soci, C.; Wang, Q. J.; Zheludev, N. I. Visible range plasmonic modes on topological insulator nanostructures. *Adv. Opt. Mater.* **2017**, *5* (3), 1600768.
(32) Glinka, Y. D.; Babakiray, S.; Johnson, T. A.; Lederman, D. Thickness tunable quantum interference between surface phonon and Dirac plasmon states in thin films of the topological insulator $Bi_2Se_3$. *J. Phys.: Condens. Matter* **2015**, *27* (5), 052203.
(33) Bansal, N.; Kim, Y. S.; Brahlek, M.; Edrey, E.; Oh, S. Thickness-independent transport channels in topological insulator $Bi_2Se_3$ thin films. *Phys. Rev. Lett.* **2012**, *109* (11), 116804.
(34) Giannini, V.; Francescato, Y.; Amrania, H.; Phillips, C. C.; Maier, S. A. Fano resonances in nanoscale plasmonic systems: A parameter-free modeling approach. *Nano Lett.* **2011**, *11* (7), 2835−2840.
(35) Francescato, Y.; Giannini, V.; Maier, S. A. Plasmonic systems unveiled by Fano resonances. *ACS Nano* **2012**, *6* (2), 1830−1838.
(36) Cao, Y.; Waugh, J. A.; Zhang, X.-W.; Luo, J.-W.; Wang, Q.; Reber, T. J.; Mo, S. K.; Xu, Z.; Yang, A.; Schneeloch, J.; Gu, G. D.; Brahlek, M.; Bansal, N.; Oh, S.; Zunger, A.; Dessau, D. S. Mapping the orbital wavefunction of the surface states in three-dimensional topological insulators. *Nat. Phys.* **2013**, *9* (8), 499−504.
(37) Yan, H.; Low, T.; Zhu, W.; Wu, Y.; Freitag, M.; Li, X.; Avouris, P.; Xia, F.; Guinea, F. Damping pathways of mid-intrared plasmons in graphene nanostructures. *Nat. Photonics* **2013**, *7* (5), 394−399.
(38) Link, S.; El-Sayed, M. A. Spectral properties and relaxation dynamics of surface plasmon electronic oscillations in gold and silver nanodots and nanorods. *J. Phys. Chem. B* **1999**, *103* (40), 8410−8426.
(39) Zhu, X.; Santos, L.; Howard, C.; Sankar, R.; Chou, F. C.; Chamon, C.; El-Batanouny, M. Electron-phonon coupling on the surface of the topological insulator $Bi_2Se_3$ determined from surface-phonon dispersion measurements. *Phys. Rev. Lett.* **2012**, *108* (18), 185501.
(40) Zhu, X.; Santos, L.; Sankar, R.; Chikara, S.; Howard, C.; Chou, F. C.; Chamon, C.; El-Batanouny, M. Interaction of phonons and Dirac fermions on the surface of $Bi_2Se_3$: A strong kohn anomaly. *Phys. Rev. Lett.* **2011**, *107* (18), 186102.
(41) Chen, J.; Badioli, M.; Alonso-González, P.; Thongrattanasiri, S.; Huth, F.; Osmond, J.; Spasenović, M.; Centeno, A.; Pesquera, A.; Godignon, P.; Elorza, A. Z.; Camara, N.; García de Abajo, F. J.; Hillenbrand, R.; Koppens, F. H. L. Optical nano-imaging of gate-tunable graphene plasmons. *Nature* **2012**, *487* (7405), 77−81.
(42) Caldwell, J. D.; Kretinin, A. V.; Chen, Y.; Giannini, V.; Fogler, M. M.; Francescato, Y.; Ellis, C. T.; Tischler, J. G.; Woods, C. R.; Giles, A. J.; Hong, M.; Watanabe, K.; Taniguchi, T.; Maier, S. A.; Novoselov, K. S. Sub-diffractional volume-confined polaritons in the natural hyperbolic material hexagonal boron nitride. *Nat. Commun.* **2014**, *5*, 5221.
(43) Dai, S.; Ma, Q.; Liu, M. K.; Andersen, T.; Fei, Z.; Goldflam, M. D.; Wagner, M.; Watanabe, K.; Taniguchi, T.; Thiemens, M.; et al. Graphene on hexagonal boron nitride as a tunable hyperbolic metamaterial. *Nat. Nanotechnol.* **2015**, *10* (8), 682−686.
(44) Fei, Z.; Scott, M. E.; Gosztola, D. J.; Foley, J. J.; Yan, J.; Mandrus, D. G.; Wen, H.; Zhou, P.; Zhang, D. W.; Sun, Y.; Guest, J. R.; Gray, S. K.; Bao, W.; Wiederrecht, G. P.; Xu, X. Nano-optical imaging of $WSe_2$ waveguide modes revealing light-exciton interactions. *Phys. Rev. B: Condens. Matter Mater. Phys.* **2016**, *94* (8), 081402.
(45) Wang, Y. H.; Hsieh, D.; Sie, E. J.; Steinberg, H.; Gardner, D. R.; Lee, Y. S.; Jarillo-Herrero, P.; Gedik, N. Measurement of intrinsic Dirac fermion cooling on the surface of the topological insulator $Bi_2Se_3$ using time-resolved and angle-resolved photoemission spectroscopy. *Phys. Rev. Lett.* **2012**, *109* (12), 127401.
(46) Valdés Aguilar, R.; Qi, J.; Brahlek, M.; Bansal, N.; Azad, A.; Bowlan, J.; Oh, S.; Taylor, A. J.; Prasankumar, R. P.; Yarotski, D. A. Time-resolved terahertz dynamics in thin films of the topological insulator $Bi_2Se_3$. *Appl. Phys. Lett.* **2015**, *106* (1), 011901.


DOI: 10.1021/acs.nanolett.7b03897
*Nano Lett.* 2018, 18, 734−739